

Molecular basis for the inhibition of human NMPRTase, a novel target for anticancer agents

Javed A Khan¹, Xiao Tao^{1,2} & Liang Tong¹

Nicotinamide phosphoribosyltransferase (NMPRTase) has a crucial role in the salvage pathway of NAD⁺ biosynthesis, and a potent inhibitor of NMPRTase, FK866, can reduce cellular NAD⁺ levels and induce apoptosis in tumors. We have determined the crystal structures at up to 2.1-Å resolution of human and murine NMPRTase, alone and in complex with the reaction product nicotinamide mononucleotide or the inhibitor FK866. The structures suggest that Asp219 is a determinant of substrate specificity of NMPRTase, which is confirmed by our mutagenesis studies. FK866 is bound in a tunnel at the interface of the NMPRTase dimer, and mutations in this binding site can abolish the inhibition by FK866. Contrary to current knowledge, the structures show that FK866 should compete directly with the nicotinamide substrate. Our structural and biochemical studies provide a starting point for the development of new anticancer agents.

NAD⁺ has important roles in many biochemical and biological processes. Its function as a cofactor in oxidation-reduction reactions is well known; NAD⁺ can also be used as a substrate in several biochemical reactions, such as those catalyzed by poly(ADP-ribose) polymerase (PARP1), sirtuins and ADP-ribosyl cyclase^{1–6}. A common feature of these biochemical reactions is that the glycosidic bond between nicotinamide and ribose in NAD⁺ is broken, destroying the parent NAD⁺ molecule and releasing free nicotinamide (NM). Therefore, these reactions could lead to a depletion of the cellular NAD⁺ pool, and NMPRTase activity is required to replenish the NAD⁺ levels by biosynthesis, salvaging the breakdown product NM and converting it to nicotinamide mononucleotide (NMN, **Fig. 1a**)⁷.

The important role of NMPRTase in NAD⁺ biosynthesis makes it an attractive target for the development of new anticancer agents^{8,9}. Tumor cells have a high rate of NAD⁺ turnover owing to elevated ADP-ribosylation activity, and NMPRTase expression is upregulated in cancers^{10,11}. Most notably, the compound FK866 potently and specifically inhibits the human NMPRTase (K_i of 0.3 nM), causes the depletion of intracellular NAD⁺ levels in tumors and ultimately induces apoptosis in these cells while having little toxicity to normal cells^{8,9,12}. FK866 also has potent antiangiogenic effects in a mouse renal-cell carcinoma model¹³. These observations suggest that inhibition of NMPRTase may provide a new approach for developing anticancer agents.

NMPRTase is functionally similar to quinolinic acid (QA) and nicotinic acid (NA, **Fig. 1a**) phosphoribosyltransferases (QAPRTase and NAPRTase), enzymes in two other NAD⁺ biosynthesis pathways. However, the amino acid sequences of the three enzymes are highly divergent (**Fig. 1b**). In addition, NMPRTase is substantially larger (by at least 100 amino acid residues) than the other two PRTases (**Fig. 1b**).

NMPRTase was originally identified as a secreted growth factor for early B cells and was named pre-B-cell colony-enhancing factor (PBEF)¹⁴. Most recently, it was found that NMPRTase is secreted by visceral fat tissues as well (it was therefore named visfatin) and may have insulin-mimetic effects¹⁵, making NMPRTase (visfatin) an interesting target for the development of new antidiabetes therapies^{15–18}. NMPRTase lacks a secretion signal sequence, and it is found in the cytoplasm and nucleus as well as extracellularly^{7,19}. How NMPRTase becomes secreted is currently not known^{7,16,19}.

Although crystal structure information is now available for QAPRTase and NAPRTase from several bacterial species^{20–22} and yeast²³, no structures are currently available for any of the NMPRTases, and it is not known how NMPRTase distinguishes between the NM and NA substrates. We set out to define the molecular mechanism for the substrate selectivity of NMPRTase and its specific inhibition by FK866. We report here the crystal structures of human and murine NMPRTase at up to 2.1-Å resolution, alone and in complex with the reaction product NMN or the potent inhibitor FK866. Our structural observations were confirmed by biochemical and mutagenesis studies and provide a foundation for the development of new anticancer agents.

RESULTS

Structure determination

The crystal structure of human NMPRTase was determined at 2.7-Å resolution by the selenomethionyl SAD method²⁴. Human NMPRTase contains only two methionine residues of a total of 490 residues (excluding the initiator methionine). We also obtained crystals of murine NMPRTase, but it contains only one methionine residue. Accordingly, the selenium anomalous signal was very small in the data

¹Department of Biological Sciences, Columbia University, New York, New York 10027, USA. ²Present address: Laboratory of Molecular Neurobiology and Biophysics, Rockefeller University, New York, New York 10021. Correspondence should be addressed to L.T. (tong@como.bio.columbia.edu).

Received 31 March; accepted 9 May; published online 18 June 2006; doi:10.1038/nsmb1105

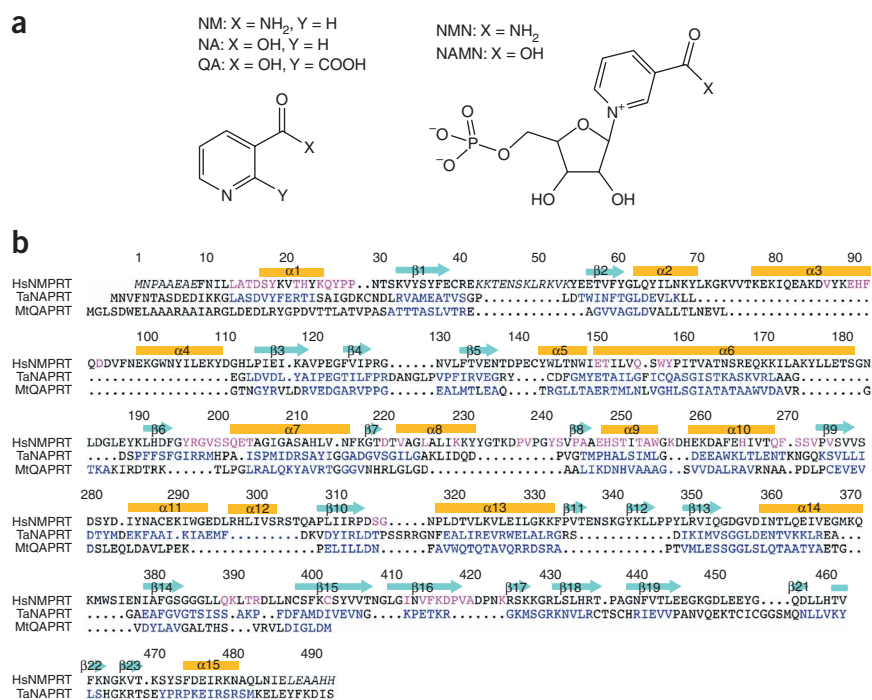


Figure 1 Sequence alignment of NMPRTase with other phosphoribosyltransferases involved in NAD⁺ biosynthesis. **(a)** Chemical structures of indicated substrates. **(b)** Structure-based sequence alignment of human NMPRTase (HsNMPRT) with NAPRTase from *T. acidophilum* (TaNAPRT)²² and QAPRTase from *M. tuberculosis* (MtQAPRT)²¹. Secondary structure elements in NMPRTase are labeled above the alignment. Blue, residues in TaNAPRT and MtQAPRT that are within 3 Å of the equivalent C α position in HsNMPRT; magenta, residues in the dimer interface of NMPRTase; dot, deletion.

collected for such selenomethionyl crystals. To increase the selenium anomalous signal, we introduced methionine residues at several positions in human NMPRTase by site-specific mutagenesis and succeeded in crystallizing the F132M I151M double mutant. Notably, the selenium anomalous signal for this mutant crystal was still very small, only about 0.2%. Nonetheless, we were able to locate the 16 selenium positions for the four NMPRTase molecules in the crystallographic asymmetric unit. After four-fold noncrystallographic symmetry (NCS) averaging, the electron density map could be readily interpreted on the basis of the amino acid sequence of NMPRTase.

To determine the binding modes of the reaction product NMN and the potent inhibitor FK866, we cocrystallized wild-type human NMPRTase with these compounds. The structures of the complexes were determined by the molecular replacement method. Clear electron density was observed for the compounds in all the NMPRTase molecules in the crystallographic asymmetric unit. The structure of the free enzyme of murine NMPRTase was determined by the molecular replacement method using the structure of human NMPRTase as the search model.

Overall structure of human NMPRTase monomer

The crystal structures of human and murine NMPRTases, alone and in complex with NMN or FK866, were determined at up to 2.1-Å resolution. The atomic models contain residues 9–41 and 54–484 of NMPRTase, and they have good agreement with the observed diffraction data and the expected bond lengths and bond angles. The majority of the residues (90%) are located in the most favored region of the Ramachandran plot. Human and murine NMPRTases share 96% amino acid sequence identity. Therefore, the structure

of the free enzyme of murine NMPRTase should also be a good model for that of human NMPRTase.

The structure of the NMPRTase monomer contains 22 β -strands and 15 α -helices (Fig. 1b) and can be divided into three domains, A, B and C (Fig. 2a). Domain A consists of a seven-stranded fully antiparallel β -sheet with five helices on one face. Residues from both the N- and C-terminal regions of NMPRTase (9–148, 391–427 and 459–484) belong to this domain. Domain B (residues 181–390) contains a seven-stranded β/α core. Helix α 6, with nine turns (residues 149–180), connects domains A and B (Fig. 2a). Domain C (residues 428–458) contains a three-stranded antiparallel β -sheet and covers the open face of the β -sheet in domain A.

The asymmetric units of these crystals contain two or six molecules of NMPRTase. The monomers in each crystal have essentially the same conformation, with r.m.s. deviation of about 0.4 Å for their equivalent C α atoms.

Structural differences to NAPRTase and QAPRTase

The overall structure of human NMPRTase shows similarity to NAPRTase and QAPRTase, despite sharing very limited sequence similarity with them. The closest structural homolog is the NAPRTase from *Thermoplasma acidophilum*²² (Fig. 2b). NMPRTase also

shows structural similarity to the QAPRTases, for example that from *Mycobacterium tuberculosis*²¹ (Fig. 2c). To facilitate structural comparisons, we have named the secondary structure elements in these enzymes using the same scheme (Fig. 1b).

There are also important conformational differences between NMPRTase and NAPRTase and QAPRTase. NMPRTase contains about 100 more amino acid residues than *T. acidophilum* NAPRTase, and the *M. tuberculosis* QAPRTase is even smaller in size. These additional residues are distributed over many regions of the structure (Fig. 1b). Most notably, the insertion of 10 residues between strand β 8 and helix α 8 in domain B of NMPRTase (Fig. 1b) has an important impact on its active site (see below).

In *T. acidophilum* NAPRTase, domain C consists of a four-stranded zinc knuckle-like structure (Fig. 2b), with four cysteine residues being the putative ligands of a zinc ion²². In comparison, domain C in NMPRTase contains only three β -strands (Fig. 2a). It does not have the zinc-knuckle fold, and it lacks any cysteine residues.

Moreover, there are differences in the orientation of domain B relative to domain A in these structures. With domain A of NMPRTase and NAPRTase placed in the same orientation, the orientation of domain B differs by about 13° between the two structures (Fig. 2b). The difference is even larger, about 34°, for the orientation of domain B in QAPRTase (Fig. 2c). These differences between the two domains have marked impact on the dimerization and the composition of the active site of these enzymes (see next section).

The dimer of human NMPRTase

Our gel-filtration and light-scattering studies show that human and murine NMPRTases are dimeric in solution. The crystal structures

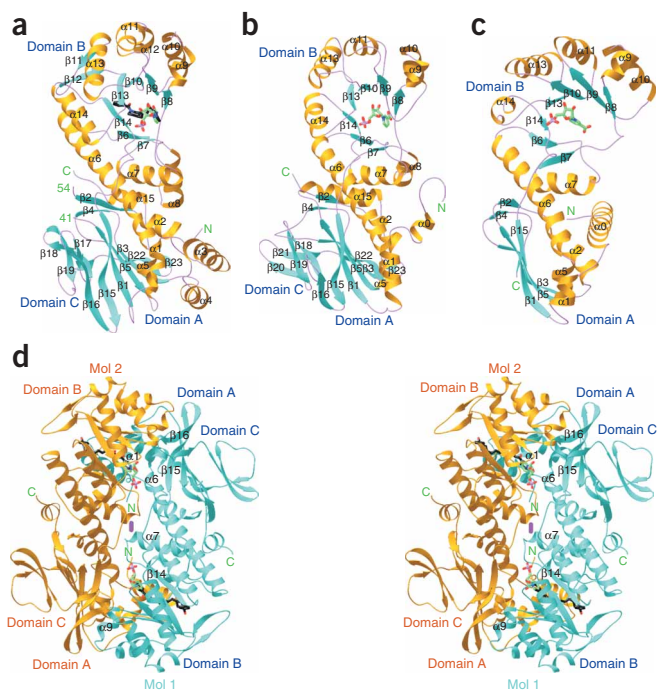


Figure 2 Structure of human NMPRTase. (a) NMPRTase monomer in complex with NMN. β -strands, α -helices and the three domains of the protein are labeled. Carbon atoms of NMN are shown in green. The bound position of FK866 is also shown (carbon atoms in black). (b) *T. acidophilum* NAPRTase in complex with NAMN²². Domain A is in the same orientation as in a. (c) *M. tuberculosis* QAPRTase in complex with NAMN²¹. (d) Stereo diagram showing the dimer of NMPRTase in complex with NMN. One monomer (Mol 1) is shown in blue, the other (Mol 2) in gold. Carbon atoms of NMN are shown in green, and those of FK866 in black. Figure was produced with Ribbons⁴⁰.

Binding mode of NMN

The active site of NMPRTase is revealed by the structure of the complex with the reaction product NMN (Fig. 3a). NMN is bound near the top of the central β -sheet in domain B (Fig. 2a). Moreover, the active site is located in the dimer interface, with several residues from the other monomer having crucial roles in recognizing the NMN molecule (Fig. 3b). Therefore, NMPRTase can be active only in its dimeric form.

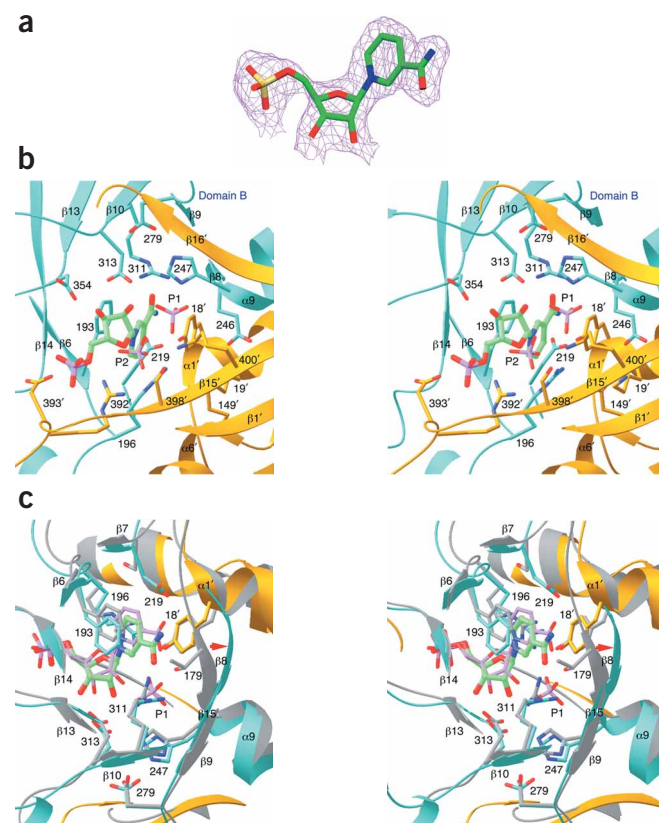
The nicotinamide ring of NMN is sandwiched between the side chain of Phe193 at the end of strand β 6 of one monomer and that of Tyr18' in helix α 1 of the other monomer (with the prime indicating the second monomer), showing π -stacking interactions (Fig. 3b). The carbonyl oxygen of the amide group of NMN is pointed toward the side chain of Arg311 (in strand β 10), although direct hydrogen bond interactions are unlikely, as the plane of the guanidinium group is perpendicular to the carbonyl group. The amide nitrogen is hydrogen bonded to the side chain of Asp219 (in β 7). The ribose and phosphate groups of NMN are located in a highly hydrophilic binding pocket, with more than ten charged residues (Fig. 3b).

reveal an intimately associated dimer for both enzymes (Fig. 2d), with 4,000 Å² of the surface area of each monomer buried at the dimer interface. The two monomers are arranged head to tail, with domain A in one monomer contacting domain B in the other monomer. Domain C is located far from the dimer interface and does not appear to help stabilize the dimer.

Residues in domain A that are in the dimer interface are located in several helices (α 1, α 3, α 5 and α 6) and two strands (β 15 and β 16) (Fig. 1b). These residues interact with those near the top of the β -sheet in domain B of the other monomer (Fig. 2d). In addition, residues in the loop connecting domains A and B (β 14- β 15 loop) are located near the two-fold axis of the dimer (Fig. 2d).

T. acidophilum NAPRTase and *M. tuberculosis* QAPRTase also use a head-to-tail arrangement to form their dimers (Supplementary Fig. 1 online). However, because of the differences in the relative positions of domains A and B in these enzymes, there are marked differences in their dimer organization compared to NMPRTase. This is especially true for QAPRTase, where helix α 1 is no longer involved in dimer formation. This has a dramatic impact on the composition of the active site of the enzymes, as a tyrosine residue in helix α 1 helps recognize the NM and NA substrates in NMPRTase and NAPRTase (see next section). Moreover, NAPRTase and QAPRTase actually exist as hexameric rings^{21,22}, whereas NMPRTase is only a dimer.

Figure 3 Binding mode of NMN and the active site of NMPRTase. (a) Final $2F_o - F_c$ electron density map for NMN at 2.2-Å resolution. The contour level is at 1 σ . Produced with Setor⁴¹. (b) Stereo diagram showing the NMN-binding site of NMPRTase. The two monomers are colored cyan and gold, respectively. NMN is shown in green, and two phosphate groups in the binding site are labeled. (c) Comparison of the binding site of NMN in NMPRTase with that of NAMN in *T. acidophilum* NAPRTase²² (gray), shown in stereo. Red arrow indicates the shift in the position of strand β 8 between the structures of NAPRTase and NMPRTase. Panels b and c were produced with Ribbons⁴⁰.



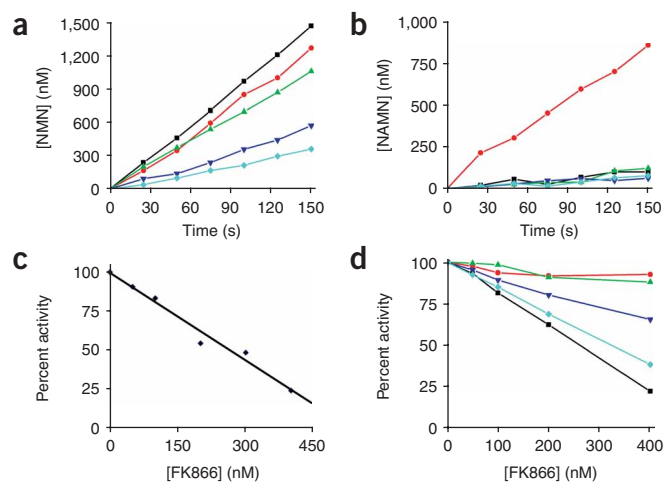


Figure 4 Kinetic characterization of substrate specificity and inhibitor sensitivity of human NMPRTase. (a) Catalytic activity of wild-type human NMPRTase (black) and D219S (red), D219N (green), H247A (blue) and R311D (cyan) mutants toward the NM substrate. (b) Catalytic activity of the same enzymes toward the NA substrate. (c) Plot of the maximal velocity of NMPRTase (obtained at 50 μ M NM) as a function of FK866 concentration. (d) Sensitivity of the wild-type human NMPRTase (black) and I309Y (red), A244M (green), S275V (blue) and I351M (cyan) mutants to FK866. Each assay in a–d has been repeated several times to ensure its reproducibility.

There are no overall conformational changes in the enzyme upon NMN binding. Most of the residues in the active site have similar conformations in the free enzyme and the NMN complex. However, the conformation of the side chains of Arg311 and Tyr18' in the free enzyme would collide with NMN (Supplementary Fig. 2 online), and structural changes in these residues may be needed for NMN binding.

Two free phosphate groups are bound near the NMN molecule (the crystallization solution contained 50 mM phosphate). The first (P1) is hydrogen bonded to the 2'-hydroxyl of NMN and to the side chains of Arg196, His247, Arg311 and Tyr18' (Fig. 3b). The second phosphate (P2) is not as ordered and interacts with the side chains of Arg196, Arg392' and Lys400' (Fig. 3b).

Molecular basis for substrate specificity

Although the overall binding mode of NMN to NMPRTase is similar to that of NAMN to *T. acidophilum* NAPRTase²², there are three major structural differences between these enzymes near the amide group of NMN (Fig. 3c). First, the side chain of the negatively charged Asp219 residue is directly hydrogen bonded to the amide group of NMN in NMPRTase (Fig. 3c), and this negative charge should disfavor the binding of NA to the active site of NMPRTase. In contrast, NAPRTases have a serine or alanine residue at the equivalent position (Fig. 1b), and its side chain is not involved in NA binding (Fig. 3c). Second, the negative charge on the carboxylate group of NA is recognized by the side chain of Arg235 in *T. acidophilum* NAPRTase (Fig. 3c). This residue is equivalent to Arg311 in NMPRTase, but it does not have optimal interactions with the amide group of NM (Fig. 3b). Finally, NMPRTase contains a 10-residue insertion in the loop connecting helix α 8 and strand β 8 (Fig. 1b). As a result, strand β 8 is shifted away by about 2 Å in NMPRTase, such that there are no direct interactions between NM and residues in this strand (Fig. 3c). This structural difference may also have crucial implications for inhibitor sensitivity (see next section).

Our mutagenesis and biochemical experiments confirm the structural observations regarding the substrate specificity of NMPRTase

(Fig. 4). We characterized the catalytic activity of the D219S, D219N, H247A and R311D mutants of NMPRTase toward the NM and NA substrates. Wild-type NMPRTase has robust activity toward the NM substrate (Fig. 4a), with a K_m value of about 2 μ M^{7,25}. The D219S and D219N mutants have roughly the same activity as the wild-type enzyme toward the NM substrate, whereas the H247A and R311D mutants have about a three-fold reduction in activity (Fig. 4a). The kinetic data are consistent with the structural information on the binding mode of NMN (Fig. 3b).

Notably, the D219S mutant has strong activity toward the NA substrate, about the same as its activity toward the NM substrate (Fig. 4b). In contrast, wild-type NMPRTase and the H247A and R311D mutants are essentially inactive with the NA substrate (Fig. 4b). Moreover, the D219N mutant is also inactive with the NA substrate, suggesting that the negative charge of Asp219 is not the sole factor disfavoring the NA substrate. In fact, the bound position of NA may be slightly different from that of NM, such that NA could clash with the bulkier Asn219 side chain (Fig. 3c). Overall, the mutagenesis and kinetic studies confirm that Asp219 is important in defining the substrate specificity of NMPRTase.

The binding mode of FK866

FK866 has clearly defined electron density from the crystallographic analysis (Fig. 5a). The compound is located in the center of the parallel β -sheet in domain B, in a tunnel at the dimer interface of NMPRTase (Fig. 5b). The pyridyl ring of the inhibitor is sandwiched between the side chains of Phe193 and Tyr18'. The carbonyl oxygen atom of the amide bond near the center of the inhibitor is hydrogen bonded to the side chain hydroxyl of Ser275 (in strand β 9), and the amide nitrogen is hydrogen bonded to a water molecule (Fig. 5c). The aliphatic carbon atoms of FK866 interact with the mostly hydrophobic side chains in the center of the β -sheet of domain B (Fig. 5b). At the other end of the inhibitor, the phenyl ring is situated in a shallow groove on the surface of NMPRTase. Only the side chains of Tyr240 and Tyr18' in this binding site show conformational changes upon inhibitor binding (Supplementary Fig. 2).

The position of the pyridyl ring of FK866 is essentially the same as that of the nicotinamide ring of NMN (Fig. 2a). Therefore, our structures predict that FK866 should be competitive against the NM substrate of the enzyme. Notably, a noncompetitive inhibition mechanism has been proposed previously on the basis of kinetic studies⁹. However, there may be a different interpretation for the kinetic data. The high potency of FK866 (K_i of 0.3 nM) suggests that it may have a very slow rate of dissociation from the enzyme, such that FK866 essentially functions as an irreversible inhibitor during the kinetic assays. Consequently, the reduction in V_{max} by the inhibitor would be due simply to the removal of active enzyme into the inactive and nondissociable enzyme–FK866 complex.

This model would predict a linear relationship between FK866 concentration and the V_{max} , $V_{max} = k_{cat}([E] - [I])$, where E and I are enzyme and inhibitor, respectively. Our kinetic data are entirely in agreement with the model (Fig. 4c). In addition, a replotting of the kinetic data reported earlier⁹ also gives a linear relationship between V_{max} and FK866 concentration (data not shown). Overall, our structural and kinetic data indicate that FK866 is a tight-binding competitive inhibitor of NMPRTase.

Molecular basis for the specificity of FK866

Our structural information reveals the molecular basis for the specificity of FK866 toward NMPRTase. The largest structural difference between NMPRTase and *T. acidophilum* NAPRTase in the

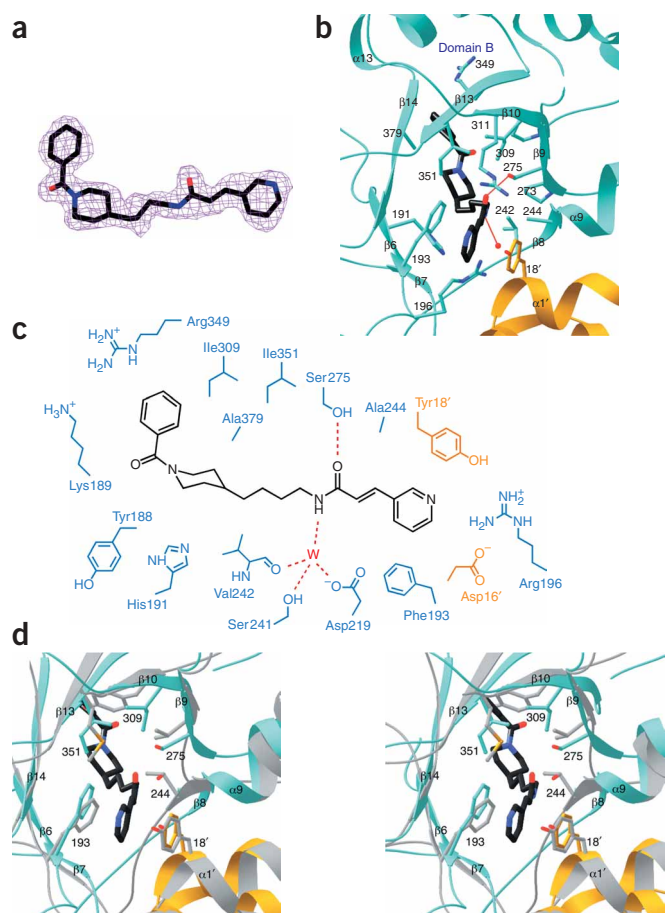


Figure 5 The FK866-binding site of human NMPRTase. **(a)** Final $2F_o - F_c$ electron density map for FK866 at 2.1-Å resolution. The contour level is at 1 σ . Produced with Setor⁴¹. **(b)** Ribbon diagram showing the FK866-binding site of NMPRTase. The two monomers are colored cyan and gold, respectively. FK866 is shown in black, and a water molecule is shown as a red sphere. Produced with Ribbons⁴⁰. **(c)** Schematic drawing of the interactions between FK866 and NMPRTase. A water molecule is shown as W in red, and hydrogen bond interactions are indicated as red dashed lines. Not shown are the hydrogen bonds between the side chains of His191 and Asp219, and Tyr18' and Arg196. **(d)** Structural comparison between NMPRTase and *T. acidophilum* NAPRTase (gray) at the FK866-binding site, shown in stereo. Produced with Ribbons⁴⁰.

importance of NAD⁺ in many nonredox reactions has become increasingly appreciated over the past few years. A common feature of these reactions is that they lead to the breakdown of NAD⁺, releasing NM. NMPRTase activity is crucial for salvaging the NM breakdown product to replenish cellular NAD⁺ levels. Our structures of human and murine NMPRTases show that they have notable overall structural similarity to NAPRTase and QAPRTase, despite sharing little sequence similarity. At the same time, detailed structural differences among these enzymes are crucial for determining their substrate specificity and inhibitor sensitivity.

Our structural and mutagenesis studies demonstrate that Asp219 is important in defining the substrate specificity of NMPRTase. However, this residue is not the sole determinant of the specificity. The D219S mutant has almost equal catalytic activity toward both the NM and NA substrates, whereas NAPRTases are inactive toward the NM substrate. Additional factors must also have important roles in defining the substrate specificity of these enzymes. Our structural analyses suggest that a possible candidate is the 10-residue insert between helix α 8 and strand β 8 in NMPRTase. In addition, differences in the dimer organization of these enzymes may also affect their substrate recognition, especially for QAPRTase.

The P1 phosphate group in the structure of the NMN complex is located next to the His247 residue (Fig. 3b). Notably, His247 is structurally equivalent to a histidine residue that is autophosphorylated in the NAPRTases²⁶. In the presence of ATP, NAPRTases catalyze the production of NAMN with concomitant hydrolysis of ATP and the formation of a phospho-histidine intermediate²⁷. Phosphorylated NAPRTase has higher catalytic activity and lower K_m for the substrates. Our structure suggests that the P1 phosphate could be a mimic for a phosphorylated His247 residue, raising the possibility that mammalian NMPRTase might also be activated by (auto)phosphorylation. Results from our kinetic assays show that the addition of free phosphate ions in the reaction buffer does not have a large impact on the activity of NMPRTase. However, our assay buffer also contained 2.5 mM ATP, which is required for one of the coupling enzymes. Further studies are needed to elucidate whether NMPRTase can be (auto)phosphorylated and whether ATP can bind the enzyme.

Our structures reveal the presence of a tunnel at the dimer interface of NMPRTase, which may be an optimal binding site for the development of potent and specific inhibitors against this enzyme. This tunnel is about 15 Å long, but it is rather narrow, with a diameter of only 6 Å in places. The slow dissociation (tight binding) behavior of FK866 could be explained by the fact that it needs to move nearly 15 Å along the tunnel to dissociate from the binding site. FK866 probably also has slow association with the enzyme. One end of the tunnel opens to the active site, and compounds bound in the tunnel can directly block the binding of the NM substrate to the enzyme. In the free enzyme, the tunnel is occupied by several water molecules. It is not known whether the tunnel has any role in catalysis by the enzyme.

FK866-binding site is for residues in strand β 8 (Fig. 5d), owing to the insertion of 10 residues in NMPRTase (Fig. 1b). This strand is placed closer to the center of the β -sheet in domain B in NAPRTase. In addition, several small residues in NMPRTase (Ala244, Ile309 and Ile351) are replaced by bulkier side chains in NAPRTase (Fig. 5d). The overall result of these sequence and structural differences is that NAPRTase does not contain a tunnel at the dimer interface, which is the molecular basis for the lack of inhibition of NAPRTases by FK866.

To examine the functional importance of our structural observations, we created mutations in the FK866-binding site and assessed their effects on the inhibitory activity of the compound (Fig. 4d). The S275V, I309Y and I351M mutations each change a residue in NMPRTase to its equivalent in *T. acidophilum* NAPRTase (Fig. 1b), and the A244M mutation would introduce substantial bulk at this position. The I309Y and A244M mutants are essentially insensitive to the FK866 compound, and the S275V mutant has reduced sensitivity to the inhibitor (Fig. 4d). In contrast, the I351M mutant has roughly the same sensitivity as the wild-type enzyme, consistent with our structural analysis showing that the methionine residue at this position in NAPRTase does not have serious steric clashes with FK866 (Fig. 5d). Overall, the results from the mutagenesis studies confirm the binding mode of FK866 and our proposed molecular mechanism for its specificity toward NMPRTase.

DISCUSSION

NAD⁺ is a central player in many cellular processes, including both redox reactions where NAD⁺ participates in hydride transfer and nonredox reactions where NAD⁺ serves as a substrate. The functional

The shape of the tunnel places severe restraints on the chemical structures of the inhibitors that can bind it. FK866 is a long, almost linear molecule and represents a good fit to this shape. Moreover, the compound has some of the pharmacophores that may be important for achieving strong interactions with this binding site. It contains an aromatic ring for π -stacking interactions with the side chains of Phe193 and Tyr18', a hydrogen bond acceptor to interact with the Ser275 side chain, and aliphatic groups that should have favorable van der Waals interactions with the mostly hydrophobic surface of the tunnel. The water molecule hydrogen bonded to the amide nitrogen of FK866 is the only solvent molecule in the tunnel in this complex. It may be entropically advantageous to displace this water by a chemical group of the inhibitor. Finally, the presence of the tunnel in only NMPRTase would ensure the specificity of inhibitors targeting this binding site.

In summary, NMPRTase is a crucial enzyme in the salvage pathway of NAD⁺ biosynthesis and has important functions in regulating NAD⁺ levels in cells undergoing substantial NAD⁺ turnover. Tumor cells have elevated NAD⁺ turnover owing to higher ADP-ribosylation activity. FK866 is a potent inhibitor of NMPRTase and can reduce NAD⁺ levels and cause apoptosis of tumor cells⁹, validating NMPRTase as a target for the development of new anticancer agents. At the same time, elevated NAD⁺ biosynthesis may protect against neurodegeneration⁵. Our studies define the three-dimensional structures of human and murine NMPRTase, elucidate the molecular mechanism for the substrate specificity of this enzyme, define the binding mode of FK866 and the structural basis for its specificity for NMPRTase, and reveal a tunnel that can be used as a binding site for inhibitors. These results provide a foundation for developing and optimizing new inhibitors against this target.

METHODS

Protein expression and purification. Full-length human and murine NMPRTase (residues 1–491) was subcloned into the pET26b vector (Novagen) and overexpressed in *Escherichia coli* at 20 °C. The expression construct introduced a His₆ tag at the C terminus. The soluble protein was purified by nickel-agarose affinity chromatography, anion exchange and gel-filtration chromatography. The protein was concentrated to 30 mg ml⁻¹ in a buffer containing 20 mM Tris (pH 7.9), 200 mM NaCl, 5 mM DTT and 5% (v/v) glycerol and stored at -80 °C. The C-terminal His tag was not removed for crystallization.

The selenomethionyl protein was produced in B834(DE3) cells (Novagen), grown in defined LeMaster media supplemented with selenomethionine (SeMet)²⁸ and purified following the same protocol as that for the native protein. To increase the selenium anomalous diffraction signal, site-specific mutants of NMPRTase were created to introduce additional methionine residues into the protein. On the basis of the sequence alignment, the following mutations were designed: L62M, I65M, F132M, I151M and I265M. The mutants were created with the QuikChange kit (Stratagene) and verified by sequencing. We screened seven different combinations of the mutation sites, as double, triple and quintuple mutants, and found that the F132M I151M double mutant could be crystallized. This double mutant was used for only the initial structure determination. Subsequent structure refinements and kinetic assays used the wild-type enzyme.

Protein crystallization. Crystals of the selenomethionyl free enzyme of human NMPRTase (F132M I151M double mutant) were grown with the sitting drop vapor diffusion method at 22 °C. The reservoir solution contained 50 mM phosphate buffer (pH 9.2), 24% (w/v) PEG 3,350, 200 mM NaCl and 5 mM DTT. BaCl₂ was used as an additive in the drop solution. The crystals were cryo-protected by transferring to the reservoir solution supplemented with 15% (v/v) ethylene glycol and flash-frozen in liquid propane for data collection at 100 K. There are four molecules of NMPRTase in the asymmetric unit.

Crystals of wild-type human NMPRTase in complex with NMN were obtained at 22 °C by sitting drop vapor diffusion. The protein (20 mg ml⁻¹) was incubated with 2 mM NMN (protein/NMN molar ratio of 1:5) at 4 °C for

30 min before crystallization setup. BaCl₂ was used as an additive in the drop solution. The reservoir solution contained 50 mM phosphate buffer (pH 9.2), 26% (w/v) PEG 3,350, 200 mM NaCl and 5 mM DTT. There are six copies of the NMPRTase–NMN complex in the asymmetric unit.

Crystals of wild-type human NMPRTase in complex with FK866 were obtained at 22 °C by sitting drop vapor diffusion. The protein (20 mg ml⁻¹) was incubated with 2 mM FK866 (protein/inhibitor molar ratio of 1:5) at 4 °C for 30 min before crystallization setup, with the same reservoir solution as for the NMN complex. There are two copies of the NMPRTase–FK866 complex in the asymmetric unit.

Crystals of wild-type murine NMPRTase free enzyme were obtained by sitting drop vapor diffusion at 4 °C, with the same reservoir solution. The crystals are isomorphous to those of the human NMPRTase–FK866 complex.

Data collection and processing. X-ray diffraction data were collected on an ADSC CCD at the X4A beamline or a Mar imaging plate detector at the X4C beamline of Brookhaven National Laboratory. A selenomethionyl SAD data set to 2.7-Å resolution was collected at 100 K on the free enzyme crystal (F132M I151M double mutant), and native reflection data sets were collected for the other crystals. The diffraction images were processed and scaled with the HKL package²⁹. The data processing statistics are summarized in **Table 1**.

Structure determination and refinement. The locations of 16 selenium atoms were determined with the program BNP³⁰. Reflection phases to 2.7-Å resolution were calculated on the basis of the SAD data with SOLVE/RESOLVE³¹, which built partial models for the four molecules of NMPRTase in the asymmetric unit.

The NCS parameters were determined on the basis of the partial models and the selenium sites, and the reflection phases were improved by four-fold NCS averaging with DM³². The atomic model for NMPRTase was built with O³³.

Table 1 Data collection and refinement statistics

	Human NMPRTase + NMN	Human NMPRTase + FK866	Free murine NMPRTase
Data collection			
Space group	<i>C</i> 2	<i>P</i> 2 ₁	<i>P</i> 2 ₁
Cell dimensions			
<i>a</i> , <i>b</i> , <i>c</i> (Å)	253.1, 101.4, 148.2	60.8, 105.9, 83.4	60.3, 107.7, 83.3
α , β , γ (°)	90, 125.5, 90	90, 96.4, 90	90, 96.6, 90
Resolution (Å)	30–2.2 (2.28–2.2)	30–2.1 (2.18–2.1)	30–2.1 (2.18–2.1)
<i>R</i> _{merge} (%)	7.3 (32.3)	9.2 (23.8)	8.1 (26.7)
<i>I</i> / σ <i>I</i>	14.6 (3.0)	11.4 (3.6)	13.5 (2.9)
Completeness (%)	96 (76)	98 (87)	95 (85)
Redundancy	2.8 (2.2)	3.3 (2.2)	3.2 (2.2)
Refinement			
Resolution (Å)	30–2.2	30–2.1	30–2.1
Number of reflections	142,302	57,137	55,602
<i>R</i> _{work} / <i>R</i> _{free} (%)	19.7 / 24.5	24.7 / 29.8	22.5 / 26.9
No. atoms			
Protein	22,214	7,431	7,416
Ligand/ion	192	58	–
Water	1,395	776	713
<i>B</i> -factors			
Protein	32.3	15.9	20.7
Ligand/ion	33.5	17.5	–
Water	33.3	23.7	27.4
R.m.s. deviations			
Bond lengths (Å)	0.006	0.009	0.009
Bond angles (°)	1.4	1.2	1.2

Numbers in parentheses are for the highest-resolution shell. One crystal was used for each data set.

After one cycle of refinement at 2.7-Å resolution with CNS³⁴, the model for the dimer of NMPRTase was used to solve the structure of the human NMPRTase–FK866 complex and the murine NMPRTase free enzyme by molecular replacement with COMO³⁵. Refinement of these structures was carried out with CNS and REFMAC³⁶. The refinement statistics are summarized in Table 1.

NMPRTase assay. All the assays were repeated several times to ensure the reproducibility of the experiments. The catalytic activity of NMPRTase was determined using a coupled-enzyme spectrometric assay, following a published protocol²⁵. Briefly, the NMN product of NMPRTase was converted to NAD⁺ with the enzyme NMN/NAMN adenyltransferase (NMNAT), and NAD⁺ was then reduced to NADH by alcohol dehydrogenase (Sigma) using ethanol as the substrate. By monitoring the appearance of NADH at 340 nm, the activity of NMPRTase could be determined. Human NMNAT was overexpressed in *E. coli* and purified following a published protocol³⁷. The reaction buffer contained 50 mM Tris (pH 7.5), 0.4 mM phosphoribosylpyrophosphate, various concentrations of NM (or NA), 2.5 mM ATP, 12 mM MgCl₂, 1.5% (v/v) ethanol, 10 mM semicarbazide (to remove the acetaldehyde product of ethanol oxidation), 0.02% (w/v) BSA, 10 μg ml⁻¹ NMNAT, 30 μg ml⁻¹ alcohol dehydrogenase and 0.5 μM NMPRTase. The reactions are carried out at room temperature.

For assays that used NA as the substrate (at 25 μM concentration), NAD synthetase (NADS, 40 μg ml⁻¹) was included to convert the nicotinic acid adenine dinucleotide product to NAD⁺ (refs. 38,39). *E. coli* NADS was overexpressed and purified following a published protocol³⁸, and NH₄Cl (2 mM) was added to the reaction buffer as the nitrogen source. The reaction buffer also contained 20 mM KCl.

Accession codes. Protein Data Bank: Coordinates have been deposited with accession codes 2GVG (human NMPRTase–NMN complex), 2GVJ (human NMPRTase–FK866 complex) and 2GVL (free murine NMPRTase).

Note: Supplementary information is available on the Nature Structural & Molecular Biology website.

ACKNOWLEDGMENTS

We thank J. Schwanof and R. Abramowitz for setting up the X4A and X4C beamlines at the National Synchrotron Light Source, Y. Shen and S. Xiang for help with data collection at the synchrotron source, M. Matsumoto, J. Buteau and D. Accili for help with the insulin assay, H. Zhang (University of Texas Southwestern Medical Center), M. Wahl (Max-Planck-Institute for Biophysical Chemistry) and S.H. Eom (Gwangju Institute of Science & Technology) for respectively providing the bacterial expression plasmids for human NMN/NAMN adenyltransferase, *E. coli* NADS and *Helicobacter pylori* NADS, and W.W. Cleland for helpful discussions. This work was supported in part by a grant from the US National Institutes of Health.

COMPETING INTERESTS STATEMENT

The authors declare that they have no competing financial interests.

Published online at <http://www.nature.com/nsmb/>

Reprints and permissions information is available online at <http://npg.nature.com/reprintsandpermissions/>

- Ziegler, M. New functions of a long-known molecule. Emerging roles of NAD in cellular signaling. *Eur. J. Biochem.* **267**, 1550–1564 (2000).
- Guarente, L. & Picard, F. Calorie restriction—the SIR2 connection. *Cell* **120**, 473–482 (2005).
- Marmorstein, R. Structure and chemistry of the Sir2 family of NAD⁺-dependent histone/protein deacetylases. *Biochem. Soc. Trans.* **32**, 904–909 (2004).
- Magni, G. *et al.* Enzymology of NAD⁺ homeostasis in man. *Cell. Mol. Life Sci.* **61**, 19–34 (2004).
- Araki, T., Sasaki, Y. & Milbrandt, J. Increased nuclear NAD biosynthesis and SIRT1 activation prevent axonal degeneration. *Science* **305**, 1010–1013 (2004).
- Guse, A.H. Second messenger function and the structure-activity relationship of cyclic adenosine diphosphoribose (cADPR). *FEBS J.* **272**, 4590–4597 (2005).
- Rongvaux, A. *et al.* Pre-B-cell colony-enhancing factor, whose expression is up-regulated in activated lymphocytes, is a nicotinamide phosphoribosyltransferase, a cytosolic enzyme involved in NAD biosynthesis. *Eur. J. Immunol.* **32**, 3225–3234 (2002).
- Wosikowski, K. *et al.* WK175, a novel antitumor agent, decreases the intracellular nicotinamide adenine dinucleotide concentration and induces the apoptotic cascade in human leukemia cells. *Cancer Res.* **62**, 1057–1062 (2002).
- Hasmann, M. & Schemainda, I. FK866, a highly specific noncompetitive inhibitor of nicotinamide phosphoribosyltransferase, represents a novel mechanism for induction of tumor cell apoptosis. *Cancer Res.* **63**, 7436–7442 (2003).
- Hufton, S.E. *et al.* A profile of differentially expressed genes in primary colorectal cancer using suppression subtractive hybridization. *FEBS Lett.* **463**, 77–82 (1999).
- van Beijnum, J.R. *et al.* Target validation for genomics using peptide-specific phage antibodies: a study of five gene products overexpressed in colorectal cancer. *Int. J. Cancer* **101**, 118–127 (2002).
- Muruganandham, M. *et al.* Metabolic signatures associated with a NAD synthesis inhibitor-induced tumor apoptosis identified by 1H-decoupled-31P magnetic resonance spectroscopy. *Clin. Cancer Res.* **11**, 3503–3513 (2005).
- Dreys, J., Loser, R., Rattel, B. & Esser, N. Antiangiogenic potency of FK866/K22.175, a new inhibitor of intracellular NAD biosynthesis, in murine renal cell carcinoma. *Anticancer Res.* **23**, 4853–4858 (2003).
- Samal, B. *et al.* Cloning and characterization of the cDNA encoding a novel human pre-B-cell colony-enhancing factor. *Mol. Cell. Biol.* **14**, 1431–1437 (1994).
- Fukuhara, A. *et al.* Visfatin, a protein secreted by visceral fat that mimics the effects of insulin. *Science* **307**, 426–430 (2005).
- Hug, C. & Lodish, H.F. Visfatin: a new adipokine. *Science* **307**, 366–367 (2005).
- Sethi, J.K. & Vidal-Puig, A. Visfatin: the missing link between intra-abdominal obesity and diabetes? *Trends Mol. Med.* **11**, 344–347 (2005).
- Stephens, J.M. & Vidal-Puig, A.J. An update on visfatin/pre-B cell colony-enhancing factor, an ubiquitously expressed, illusive cytokine that is regulated in obesity. *Curr. Opin. Lipidol.* **17**, 128–131 (2006).
- Kitani, T., Okuno, S. & Fujisawa, H. Growth phase-dependent changes in the subcellular localization of pre-B-cell colony-enhancing factor. *FEBS Lett.* **544**, 74–78 (2003).
- Eads, J.C., Ozturk, D., Wexler, T.B., Grubmeyer, C. & Sacchettini, J.C. A new function for a common fold: the crystal structure of quinolinic acid phosphoribosyltransferase. *Structure* **5**, 47–58 (1997).
- Sharma, V., Grubmeyer, C. & Sacchettini, J.C. Crystal structure of quinolinic acid phosphoribosyltransferase from *Mycobacterium tuberculosis*: a potential TB drug target. *Structure* **6**, 1587–1599 (1998).
- Shin, D.H. *et al.* Crystal structure of a nicotinate phosphoribosyltransferase from *Thermoplasma acidophilum*. *J. Biol. Chem.* **280**, 18326–18335 (2005).
- Chappie, J.S. *et al.* The structure of a eukaryotic nicotinic acid phosphoribosyltransferase reveals structural heterogeneity among type II PRtases. *Structure* **13**, 1385–1396 (2005).
- Hendrickson, W.A. Determination of macromolecular structures from anomalous diffraction of synchrotron radiation. *Science* **254**, 51–58 (1991).
- Revollo, J.R., Grimm, A.A. & Imai, S.-I. The NAD biosynthesis pathway mediated by nicotinamide phosphoribosyltransferase regulates Sir2 activity in mammalian cells. *J. Biol. Chem.* **279**, 50754–50763 (2004).
- Gross, J., Rajavel, M., Segura, E. & Grubmeyer, C. Energy coupling in *Salmonella typhimurium* nicotinic acid phosphoribosyltransferase: identification of His-219 as site of phosphorylation. *Biochemistry* **35**, 3917–3924 (1996).
- Gross, J.W., Rajavel, M. & Grubmeyer, C. Kinetic mechanism of nicotinic acid phosphoribosyltransferase: implications for energy coupling. *Biochemistry* **37**, 4189–4199 (1998).
- Hendrickson, W.A., Horton, J.R. & LeMaster, D.M. Selenomethionyl proteins produced for analysis by multiwavelength anomalous diffraction (MAD): a vehicle for direct determination of three-dimensional structure. *EMBO J.* **9**, 1665–1672 (1990).
- Otwinowski, Z. & Minor, W. Processing of X-ray diffraction data collected in oscillation mode. *Methods Enzymol.* **276**, 307–326 (1997).
- Weeks, C.M. & Miller, R. The design and implementation of SnB v2.0. *J. Appl. Crystallogr.* **32**, 120–124 (1999).
- Terwilliger, T.C. SOLVE and RESOLVE: automated structure solution and density modification. *Methods Enzymol.* **374**, 22–37 (2003).
- Collaborative Computational Project, Number 4. The CCP4 suite: programs for protein crystallography. *Acta Crystallogr. D Biol. Crystallogr.* **50**, 760–763 (1994).
- Jones, T.A., Zou, J.Y., Cowan, S.W. & Kjeldgaard, M. Improved methods for building protein models in electron density maps and the location of errors in these models. *Acta Crystallogr. A* **47**, 110–119 (1991).
- Brunger, A.T. *et al.* Crystallography & NMR System: a new software suite for macromolecular structure determination. *Acta Crystallogr. D Biol. Crystallogr.* **54**, 905–921 (1998).
- Jogl, G., Tao, X., Xu, Y. & Tong, L. COMO: a program for combined molecular replacement. *Acta Crystallogr. D Biol. Crystallogr.* **57**, 1127–1134 (2001).
- Murshudov, G.N., Vagin, A.A. & Dodson, E.J. Refinement of macromolecular structures by the maximum-likelihood method. *Acta Crystallogr. D Biol. Crystallogr.* **53**, 240–255 (1997).
- Zhou, T. *et al.* Structure of human nicotinamide/nicotinic acid mononucleotide adenyltransferase. Basis for the dual substrate specificity and activation of the oncolytic agent tiazofurin. *J. Biol. Chem.* **277**, 13148–13154 (2002).
- Jauch, R., Humm, A., Huber, R. & Wahl, M.C. Structures of *Escherichia coli* NAD synthetase with substrates and products reveal mechanistic rearrangements. *J. Biol. Chem.* **280**, 15131–15140 (2005).
- Kang, G.B. *et al.* Crystal structure of NH₃-dependent NAD⁺ synthetase from *Helicobacter pylori*. *Proteins* **58**, 985–988 (2005).
- Carson, M. Ribbon models of macromolecules. *J. Mol. Graph.* **5**, 103–106 (1987).
- Evans, S.V. SETOR: hardware lighted three-dimensional solid model representations of macromolecules. *J. Mol. Graph.* **11**, 134–138 (1993).